

Spin-lattice model simulations of tetragonal FePt system

Jakub Šebesta^{1,*} and Dominik Legut^{2,1}

¹*IT4Innovations, VSB – Technical University of Ostrava,
17. listopadu 2172/15, 708 00 Ostrava, Czech Republic*

²*Charles University, Faculty of Mathematics and Physics Ke Karlovu 3, 121 16 Praha 2, Czech Republic*

(Dated: January 13, 2026)

Magnetic materials play a key role in the contemporary industry, providing unique features with a wide application potential. To study physical phenomena and design new materials, it is important to possess an appropriate tool, a model allowing simulation of desired behavior. Spin-lattice model simulations can be used to investigate spacious systems containing thousands of atoms, while complex phenomena arising from the interplay of lattice and spin dynamics can be modeled. One of the important phenomena that can be modeled in the spin lattice simulation is magnetoelastic behavior, offering direct conversion between the mechanical and magnetic energy. However, so far, only models for systems with cubic symmetry have been introduced. Therefore, here, a spin-lattice model for a system with tetragonal symmetry is proposed, where its strength is manifested by simulation of magnetoelastic properties of a characteristic representative L1₀ FePt system.

I. INTRODUCTION

Magnetic materials are widely used in daily life, however simulations of their behavior are much more complicated than for the non-magnetic systems. For certain physical phenomena, the magnetic and elastic properties cannot be treated separately as the interplay between magnetic and mechanical degrees of freedom plays a vital role. Such coupling is called magnetoelasticity merging magnetic and elastic properties of the system [1, 2]. It is manifested, e.g., in axial or volume magnetostriction and it allows a conversion between magnetic and mechanical energy which is employed in various sensors and actuators e.g., torque sensors, fuel injectors, micro-pump, weak-field detectors etc. [3–9].

To simulate the magnetoelastic coupling, distinct methods can be used depending on the system size. For small systems, a method combining atomistic spin dynamics and ab-initio molecular dynamics (ASD-AIMD) [10] might be used. However, such an approach became computationally demanding for large system based on a spacious supercell, where the spin-lattice (SL) model [11, 12] based simulations take place. The SL model considers at once the spin and lattice degrees of freedom. The SL dynamics is governed by a Hamiltonian considering together the interatomic potential, magnetic interactions, such as the Heisenberg or dipole-dipole interactions, magnetocrystalline anisotropy, etc. The SL model offers a modeling system behavior in time and at finite temperature, which allows one to study e.g., magnon-phonon interactions, ultra-fast demagnetization processes, and energy flows in the lattice and spin subsystems.

The SL model has been successfully employed for a description of magnetoelastic behavior of ferromagnetic (FM) cubic systems [13–15]. However, their magneto-

lastic behavior is weak [16]. Much stronger magnetoelastic response can be observed in tetragonal systems due to the symmetry, as for L1₀ FePt system [17] possessing substantial magnetocrystalline anisotropy [17, 18]. Therefore, in this paper, the spin-lattice model description for the tetragonal symmetry is derived. The SL model is applied to simulate the magnetoelastic behavior of the tetragonal FePt system.

II. THEORY AND METHODOLOGY

For magnetic systems, besides the elastic energy E_{el} , magnetoelastic energy E_{me} describing the interplay between the magnetic and mechanical degrees of freedom has to be taken into account. Regarding the tetragonal (I) symmetry, the magnetoelastic energy in Cartesian reads [19]

$$\begin{aligned} \frac{1}{V_0} E_{me} = & b_{11}(\varepsilon_{xx} + \varepsilon_{yy}) + b_{12}\varepsilon_{zz} \\ & + b_{21}(\alpha_z^2 - \frac{1}{3})(\varepsilon_{xx} + \varepsilon_{yy}) + b_{22}(\alpha_z^2 - \frac{1}{3})\varepsilon_{zz} \\ & + \frac{1}{2}b_3(\alpha_x^2 - \alpha_y^2)(\varepsilon_{xx} - \varepsilon_{yy}) + 2b'_3\alpha_x\alpha_y\varepsilon_{xy} \\ & + 2b_4(\alpha_x\alpha_z\varepsilon_{xz} + \alpha_y\alpha_z\varepsilon_{yz}), \end{aligned} \quad (1)$$

where ε_{ij} denotes components of strain tensor ε , α_i stands for Cartesian components of the magnetization directions ($|\alpha| = 1$) and b_i represents magnetetoelastic constants, where the b_{11} and b_{12} constants are related to the isotropic volume, the rest of them describes the anisotropic behavior.

Considering the elastic energy E_{el} for the tetragonal

* jakub.sebesta@vsb.cz

(I) symmetry [20]

$$\begin{aligned} \frac{1}{V_0}(E_{\text{el}} - E_0) &= \quad (2) \\ &= \frac{1}{2}C_{11}(\tilde{\varepsilon}_1^2 + \tilde{\varepsilon}_2^2) + C_{12}\tilde{\varepsilon}_1\tilde{\varepsilon}_2 + C_{13}(\tilde{\varepsilon}_1 + \tilde{\varepsilon}_2)\tilde{\varepsilon}_3 \\ &+ \frac{1}{2}C_{33}\tilde{\varepsilon}_3^2 + \frac{1}{2}C_{44}\tilde{\varepsilon}_4^2 + \tilde{\varepsilon}_5^2 + \frac{1}{2}C_{66}\tilde{\varepsilon}_6 \\ &= \frac{1}{2}c_{xxxx}(\varepsilon_{xx}^2 + \varepsilon_{yy}^2) + c_{xxyy}(\varepsilon_{xx}\varepsilon_{yy}) + c_{xxzz}(\varepsilon_{xx} + \varepsilon_{yy})\varepsilon_{zz} \\ &+ \frac{1}{2}c_{zzzz}\varepsilon_{zz}^2 + 2c_{yzyz}(\varepsilon_{yz}^2 + \varepsilon_{zx}^2) + 2c_{xyxy}\varepsilon_{xy}, \end{aligned}$$

and the equilibrium strain is defined as follows

$$\frac{\partial E_{\text{el}} + E_{\text{me}}}{\partial \varepsilon_{ij}^{\text{eq}}} = 0, \quad (3)$$

the magnetostriction described by the relative length change $\Delta l/l_0$ along the direction $\boldsymbol{\nu}$ for the magnetization direction $\boldsymbol{\alpha}$ reads

$$\begin{aligned} \frac{\Delta l}{l_0} \bigg|_{\boldsymbol{\nu}}^{\boldsymbol{\alpha}} &= \lambda^{\alpha 1,0}(\nu_x^2 + \nu_y^2) + \lambda^{\alpha 2,0}\nu_z^2 \quad (4) \\ &+ \lambda^{\alpha 1,2}(\alpha_z^2 - \frac{1}{3})(\nu_x^2 + \nu_y^2) + \lambda^{\alpha 2,2}(\alpha_z^2 - \frac{1}{3})\nu_z^2 \\ &+ \frac{1}{2}\lambda^{\gamma,2}(\alpha_z^2 - \alpha_y^2)(\nu_x^2 - \nu_y^2) + 2\lambda^{\delta,2}\alpha_x\alpha_y\nu_x\nu_y \\ &+ 2\lambda^{\varepsilon,2}(\alpha_x\alpha_z\nu_x\nu_z + \alpha_y\alpha_z\nu_y\nu_z), \end{aligned}$$

where λ^i denotes magnetostrictive coefficients. Similarly to the magnetolelastic constants b_i , the isotropic $\lambda^{\alpha 1,0}$ and $\lambda^{\alpha 1,0}$ coefficients belong to the the volume magnetostriction [21]

$$\lambda^{\alpha 1,0} = \frac{-b_{11}C_{33} + b_{12}C_{13}}{C_{33}(C_{11} + C_{12}) - 2C_{13}^2}, \quad (5)$$

$$\lambda^{\alpha 2,0} = \frac{2b_{11}C_{13} - b_{12}(C_{11} + C_{12})}{C_{33}(C_{11} + C_{12}) - 2C_{13}^2}. \quad (6)$$

The remaining ones are anisotropic coefficients related to the magnetization direction-dependent magnetostriction [19]

$$\lambda^{\alpha 1,2} = \frac{-b_{21}C_{33} + b_{22}C_{13}}{C_{33}(C_{11} + C_{12}) - 2C_{13}^2} \quad (7)$$

$$\lambda^{\alpha 2,2} = \frac{2b_{21}C_{13} - b_{22}(C_{11} + C_{12})}{C_{33}(C_{11} + C_{12}) - 2C_{13}^2} \quad (8)$$

$$\lambda^{\gamma,2} = \frac{-b_3}{C_{11} - C_{12}} \quad (9)$$

$$\lambda^{\delta,2} = \frac{-b'_3}{2C_{66}} \quad (10)$$

$$\lambda^{\varepsilon,2} = \frac{-b_4}{2C_{44}}. \quad (11)$$

To model the magnetoelastic behavior of tetragonal systems, a spin-lattice Hamiltonian H_{SL} with terms similar to the cubic model [12, 13] can be considered. It reads

$$\mathcal{H}_{SL}(\mathbf{r}, \mathbf{p}, \boldsymbol{\alpha}) = \sum_{i=1}^N \frac{\mathbf{p}_i}{2m_i} + \sum_{i,j=1}^N \mathcal{V}_{ij}(r_{ij}) + \mathcal{H}_M(\mathbf{r}, \boldsymbol{\alpha}), \quad (12)$$

where \mathbf{r}_i , \mathbf{p}_i , denotes the position, momentum of an atom i with the mass m_i , N is total number of atom, $\mathcal{V}_{ij}(r_{ij})$ represents the interatomic potential dependent on the atom distance $r = |\mathbf{r}_i - \mathbf{r}_j|$ and magnetic interactions are described by the Hamiltonian \mathcal{H}_M . It includes the Zeeman term for the interaction with the external magnetic field, magnetic exchange interaction of classical spins, pseudo-dipolar interaction, and tetragonal magnetocrystalline anisotropy (MCA) to include effects arising from spin-orbit coupling [12]:

$$\begin{aligned} \mathcal{H}_M(\mathbf{r}, \boldsymbol{\alpha}) &= \quad (13) \\ &= \mathcal{H}_Z(\boldsymbol{\alpha}) + \mathcal{H}_{\text{ex}}(\mathbf{r}, \boldsymbol{\alpha}) + \mathcal{H}_{\text{di}}(\mathbf{r}, \boldsymbol{\alpha}) + \mathcal{H}_{\text{MCA}}(\boldsymbol{\alpha}) \\ &- \mu_0 \sum_{i=1}^N \mu_i \mathbf{H} \cdot \boldsymbol{\alpha}_i - \frac{1}{2} \sum_{\substack{i,j=1 \\ i \neq j}}^N J_{ij}(r_{ij}) \boldsymbol{\alpha}_i \cdot \boldsymbol{\alpha}_j \\ &- \frac{1}{2} \sum_{i,j=1}^N l_{ij}(r_{ij}) \left[(\mathbf{e}_{ij} \cdot \boldsymbol{\alpha}_i)(\mathbf{e}_{ij} \cdot \boldsymbol{\alpha}_j) - \frac{(\boldsymbol{\alpha}_i \cdot \boldsymbol{\alpha}_j)}{3} \right] \\ &+ \left[K_1 \sin^2(\theta) + K_2 \sin^4(\theta) + K_3 \sin^4(\theta) \cos(4\phi) \right]; \\ \mathbf{e}_{ij} &= \frac{\mathbf{r}_{ij}}{r_{ij}}, \end{aligned} \quad (14)$$

where μ_0 is the permeability of vacuum, μ_i denotes magnetic moment of the atom i , H is an external magnetic field, $J_{ij}(r_{ij})$ stands for magnetic exchange coupling, $l(r_{ij})$ is a parameter of the pseudo-dipolar interaction, K_i denotes magnetocrystalline anisotropy constants, θ is the angle between the spin direction $\boldsymbol{\alpha}$ and tetragonal axes c ($c \neq a = b$), and ϕ is an angle in the basal ab -plane between the spin direction $\boldsymbol{\alpha}$ and tetragonal axes a .

Performing the simulations within the LAMMPS package [11, 12, 22], the radial dependence of the exchange interaction coupling $J_{ij}(r_{ij})$ and the pseudo-dipolar coupling $l(r_{ij})$ can be parametrized by a Bethe-Slater curve $\Phi(r_{ij})$ [12]:

$$\Phi(r_{ij}) = 4\alpha \left(\frac{r_{ij}}{\delta} \right)^2 \left[1 - \gamma \left(\frac{r_{ij}}{\delta} \right)^2 \right] e^{-\left(\frac{r_{ij}}{\delta} \right)^2} \Theta(R_c - r_{ij}), \quad (15)$$

where α , γ , δ are parameters, and $\Theta(R_c - r_{ij})$ denotes the Heaviside step function with the radial cut-off R_c .

The anisotropic part of the magnetoelastic energy (Eq. 1) can be included in the spin-lattice model Hamiltonian (Eq. 12) via the pseudo-dipolar term \mathcal{H}_{di} (Eq. 13)

$$\mathcal{H}_{di}(\mathbf{r}, \boldsymbol{\alpha}) = \quad (16)$$

$$= -\frac{1}{2} \sum_{i,j=1}^N l_{ij}(r_{ij}) \left[(\mathbf{e}_{ij} \cdot \boldsymbol{\alpha}_i)(\mathbf{e}_{ij} \cdot \boldsymbol{\alpha}_j) - \frac{(\boldsymbol{\alpha}_i \cdot \boldsymbol{\alpha}_j)}{3} \right],$$

whereas the isotropic part can be modeled by the exchange interaction \mathcal{H}_{ex} .

For FM ordered spins ($\boldsymbol{\alpha}_i \cdot \boldsymbol{\alpha}_j = 1$), the pseudo-dipolar term \mathcal{H}_{di} is simplified as follows:

$$\mathcal{H}_{di}^{\parallel}(\mathbf{r}, \boldsymbol{\alpha}) = -\frac{1}{2} \sum_{i,j=1}^N l_{ij}(r_{ij}) \left[(\mathbf{e}_{ij} \cdot \boldsymbol{\alpha}_i)^2 - \frac{1}{3} \right]. \quad (17)$$

Considering pseudo-dipolar interaction between various neighbors and its change under small deformations, the

behavior of the tetragonal (I) magnetoelastic energy (Eq. 1) can be reconstructed. To simplify the model and include only the magnetization direction dependent term in the magnetoelastic energy (Eq. 1), the following form of the pseudo-dipolar interaction is considered:

$$\tilde{\mathcal{H}}_{di}(\mathbf{r}, \mathbf{s}) = \quad (18)$$

$$= -\frac{1}{2} \sum_{i,j=1}^N l_{ij}(r_{ij}) \left[(\mathbf{e}_{ij} \cdot \boldsymbol{\alpha}_i)(\mathbf{e}_{ij} \cdot \boldsymbol{\alpha}_j) - \frac{(\boldsymbol{\alpha}_i \cdot \boldsymbol{\alpha}_j)}{3} + \frac{1}{3} \right].$$

Assuming tetragonal (I) structure with a single atom in the primitive cell, FM ordered spins, and pseudo-dipolar interactions $\tilde{\mathcal{H}}_{di}$ (Eq. 18) up to the fourth-nearest neighboring atoms (Fig. 1), the change of pseudo-dipolar Hamiltonian $\Delta\tilde{\mathcal{H}}_{di}$ under small deformations, represented by the strain tensor $\boldsymbol{\varepsilon}$, can be approximate as follows:

$$-\Delta\tilde{\mathcal{H}}_{di}(\mathbf{r}, \boldsymbol{\alpha}, \boldsymbol{\varepsilon}) = \quad (19)$$

$$\begin{aligned} &= l_1(r_{01}) 2 \left[2\alpha_x \alpha_y \varepsilon_{xy} + \alpha_x \alpha_z \varepsilon_{xz} + \alpha_y \alpha_z \varepsilon_{yz} \right] + r_{01} \frac{\partial l_1}{\partial r} \Big|_{r=r_{01}} \left[\alpha_x^2 \varepsilon_{xx} + \alpha_y^2 \varepsilon_{yy} \right] \\ &+ l_2(r_{02}) 2 \left(\alpha_x \alpha_z \varepsilon_{xz} + \alpha_y \alpha_z \varepsilon_{yz} \right) + r_{02} \frac{\partial l_2}{\partial r} \Big|_{r=r_{02}} \alpha_z^2 \varepsilon_{zz} \\ &+ l_3(r_{03}) 2 \left[\alpha_x^2 \varepsilon_{xx} + \alpha_y^2 \varepsilon_{yy} + 2\alpha_x \alpha_y \varepsilon_{xy} + \alpha_x \alpha_z \varepsilon_{xz} + \alpha_y \alpha_z \varepsilon_{yz} \right] \\ &+ r_{03} \frac{\partial l_3}{\partial r} \Big|_{r=r_{03}} \left[\alpha_x^2 \varepsilon_{xx} + \alpha_x^2 \varepsilon_{yy} + \alpha_y^2 \varepsilon_{xx} + \alpha_y^2 \varepsilon_{yy} + 4\alpha_x \alpha_y \varepsilon_{xy} \right] \\ &+ l_4(r_{04}) \frac{4}{w^2} \left[\alpha_x^2 \varepsilon_{xx} + \alpha_y^2 \varepsilon_{yy} + 2\alpha_x \alpha_y \varepsilon_{xy} + \alpha_x \alpha_z \varepsilon_{xz} (2k^2 + 1) + \alpha_y \alpha_z \varepsilon_{yz} (2k^2 + 1) + 2\alpha_z^2 \varepsilon_{zz} k^2 \right] \\ &+ r_{04} \frac{\partial l_4}{\partial r} \Big|_{r=r_{04}} \frac{2}{w^2} \left[\alpha_x^2 \varepsilon_{xx} + \alpha_y^2 \varepsilon_{yy} + k^2 \left(4\alpha_x \alpha_z \varepsilon_{xz} + 4\alpha_y \alpha_z \varepsilon_{yz} \alpha_z^2 \varepsilon_{xx} + \alpha_z^2 + \alpha_z^2 \varepsilon_{zz} (2k^2 - 1) + \varepsilon_{zz} \right) \right]; \\ &k = \frac{c}{a}, w^2 = (k^2 + 1) \end{aligned} \quad (20)$$

where $l_i(r_i)$ denotes pseudo-dipolar interaction coupling between i^{th} nearest neighbors, r_{0i} represents undeformed bond length r_i , and a resp. c are tetragonal lattice parameters.

Comparing the changes in the pseudo-dipolar interaction under small deformations (Eq. 19) to the form of the tetragonal magnetoelastic energy (Eq. 1), the dipolar interaction coupling $l_i(r_i)$ can be expressed in terms of the magnetoelastic constants b_i in following way

$$l_1(r_{01}) = -\frac{1}{2} b'_3 - \frac{1}{8} b_3 \quad , \quad (21)$$

$$r_{01} \frac{\partial l_1}{\partial r} \Big|_{r=r_{01}} = -b_3 + \frac{4}{w^2 k^2} b_{21} \quad , \quad (22)$$

$$l_2(r_{02}) = -b_4 + \frac{1}{2} b'_3 + \frac{8}{w^2} b_{21} \quad , \quad (23)$$

$$r_{02} \frac{\partial l_2}{\partial r} \Big|_{r=r_{02}} = -b_{22} + \frac{4(2k^2 - 1)}{w^2} b_{21} \quad , \quad (24)$$

$$l_3(r_{03}) = 0, \quad (25)$$

$$r_{03} \frac{\partial l_3}{\partial r} \Big|_{r=r_{03}} = \frac{1}{4} b_3, \quad (26)$$

$$l_4(r_{04}) = 0, \quad (27)$$

$$r_{04} \frac{\partial l_4}{\partial r} \Big|_{r=r_{04}} = -\frac{2w^2}{k^2} b_{21}, \quad (28)$$

where mutual interrelations between the change of the bond length r_i were taken into account. Assuming a primitive tetragonal $2 \times 2 \times 2$ supercell (Fig. 1), each type of pseudo-dipolar interaction l_i can be attributed to specific pairs of interacting atoms. Then, regarding LAMMPS simulations, a pseudo-dipolar interaction $l_i(r_i)$ can be parametrized by a Bethe-Slater curve $\Phi_{l,i}(r_i)$ (Eq. 15) where

$$\alpha_{l,i} = \frac{e}{8} \left[2l_i(r_{0i}) - r_{0i} \frac{\partial l_i}{\partial r} \Big|_{r=r_{0i}} \right], \quad (29)$$

$$\gamma_{l,i} = \frac{r_{0i} \frac{\partial l_i}{\partial r} \Big|_{r=r_{0i}}}{r_{0i} \frac{\partial l_i}{\partial r} \Big|_{r=r_{0i}} - 2l_i(r_{0i})}, \quad (30)$$

$$\delta_{l,i} = r_{0i}, \quad (31)$$

and the radial cut-off $R_{c,l,i}$ is set to include only the nearest neighbors of the selected kind of interacting atoms.

As the derived strain induced difference in pseudo-dipolar interaction (Eq. 19) contains a magnetization direction independent term $r_{04} \frac{\partial l_4}{\partial r} \Big|_{r=r_{04}} \frac{2k^2}{w^2} \varepsilon_{zz}$, an extra interaction \mathcal{H}_{off} was introduced in the model to offset this term:

$$\mathcal{H}_{\text{off}}(\mathbf{r}) = -\frac{1}{2} \sum_{i,j=1}^N l_{ij}^{\text{off}}(r_{ij}), \quad (32)$$

where

$$l_2^{\text{off}}(r_{02}) = 0, \quad (33)$$

$$r_{02} \frac{\partial l_2^{\text{off}}}{\partial r} \Big|_{r=r_{02}} = \frac{4}{w^2} b_{21}. \quad (34)$$

For better feasibility of the model spin-lattice model, the magnetocrystalline anisotropy \mathcal{H}_{MCA} can be written as follows

$$\mathcal{H}_{\text{MCA}}(\boldsymbol{\alpha}) = K_1 \left[1 - (\boldsymbol{\alpha} \cdot \mathbf{n}_c)^2 \right] \quad (35)$$

$$+ \left[1 - (\boldsymbol{\alpha} \cdot \mathbf{n}_c)^2 \right]^2 \left[K_2 + K_3 \left[8(\boldsymbol{\alpha} \cdot \mathbf{n}_a)^4 - 8(\boldsymbol{\alpha} \cdot \mathbf{n}_a)^2 + 1 \right] \right];$$

$$|\mathbf{n}_c| = |\mathbf{n}_a| = 1$$

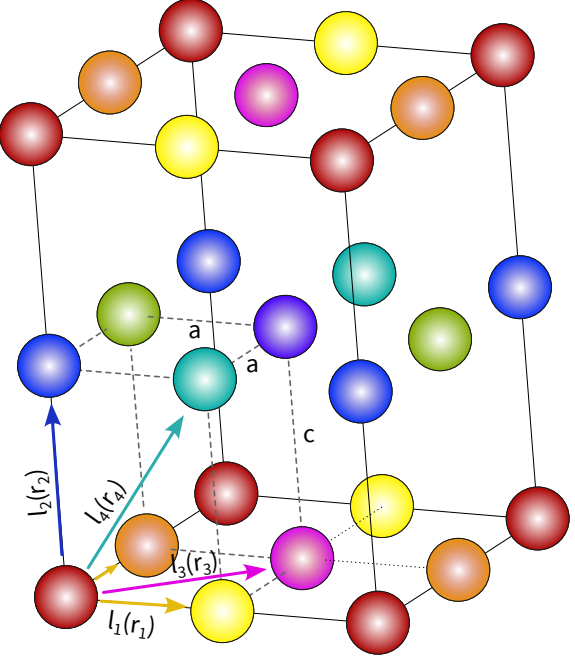


FIG. 1. Tetragonal supercell $2 \times 2 \times 2$ with depicted pseudo-dipolar interactions $l_i(r_i)$

TABLE I. Elastic properties of L1_0 FePt obtained either by ab-initio VASP calculation or spin-lattice simulation in LAMMPS. Lattice parameters a and c relaxed by DFT calculations. Equilibrium volumes in the SL simulations are determined from the energy volume curves (Fig 2).

	VASP PBE+SO	LAMMPS		
		MEAM	RF-MEAM	RF-MEAM + SL model
$a(\text{\AA})$	2.723			
$a(\text{\AA})$	3.768			
$V(\text{\AA}^3)$	27.937	26.711	27.952	27.946
$C_{11}(\text{GPa})$	374.6	353.5	365.7	365.6
$C_{12}(\text{GPa})$	81.4	185.2	85.1	85.1
$C_{13}(\text{GPa})$	154.9	195.0	157.5	157.7
$C_{33}(\text{GPa})$	299.4	245.3	299.4	300.8
$C_{44}(\text{GPa})$	109.5	103.3	108.8	108.9
$C_{66}(\text{GPa})$	49.7	35.7	56.8	56.9
$B(\text{GPa})$	203.4	233.6	203.4	203.7

where \mathbf{n}_c resp. \mathbf{n}_a denote directions of the tetragonal c -resp. a -axis. Comparing the pseudo-dipolar interaction (Eq. 17) to the above expression of the MAE (Eq. 35), it is straightforward that the pseudo-dipolar interaction contributes to the MAE, namely the K_1 term. Therefore, the value of K_1 parameter in the SL model has to be corrected for the contribution of the pseudo-dipolar coupling. Then, the adjusted \tilde{K}_1 parameter reads

$$\tilde{K}_1 = K_1 + 2 \left(l_1(r_{01}) - l_2(r_{02}) + l_3(r_{03}) \right) - \frac{4l_4(r_{04})}{w^2} \quad (36)$$

III. CALCULATION DETAILS

Background ab-initio calculations, including structure relaxation and calculation of magnetocrystalline anisotropy energy (MAE), elastic and magnetoelastic parameters used for setting the numerical parameters of the spin lattice-model were done within Vienna ab-initio simulation package (VASP) [23, 24] employing projector-augmented-wave (PAW) method with PAW pseudo-potentials. Non-collinear spin calculations including spin-orbit coupling consider the generalized gradient approximation (GGA) of Perdew-Burke-Ernzerhof (PBE) [25] with the plane wave cut-off of 450 eV for the MAE and elastic constants calculations, resp. 520 eV in case of the magnetoelastic parameters. Non-spherical contributions to the gradient corrections were included. Calculations were performed on an automatic k -mesh with $R_k = 70$ by tetrahedron Brillouin zone integration, except for magnetoelastic parameters, while higher $R_k = 130$ and Methfessel-Paxton scheme with a smearing 0.01 eV was employed. The same energy smearing was used for the structure relaxation. In general, energy convergence better than 10^{-6} eV was considered. Regarding MAE and magnetoelastic parameters more accurate convergence better than 10^{-9} eV was required. The elastic and magnetoelastic parameters were estimated by a finite displacements method employing AELAS [20] and MEALAS [16] packages, serving for the generation of distorted structures, including the spin direction for magnetoelastic constants, and data analysis.

Besides, the Relativistic Spin Polarized toolkit (RSPt)

TABLE II. Bethe-Slater curve parameters for pseudo-dipolar interactions $l_i(r_i)$, $l_i^{\text{off}}(r_i)$. The parameters are related to magnetoelastic behavior depicted in the Figure 6. The pseudo-dipolar interaction is applied only to the Fe sublattice in the presented SL model.

	α (meV)	γ	δ (Å)
SL model without the l_4 interaction			
l_1	-5.087232	0.146938	2.722735
l_2	7.146105	-0.372690	3.768487
l_3	0.186877	1.000000	3.850528
SL model with only the l_4 interaction			
l_4	15.079223	1.000000	4.649170
l_2^{off}	-6.795979	1.000000	3.768487
SL model with all l_i interactions			
l_1	-8.634783	0.497414	2.722735
l_2	15.088129	-1.451815	3.768487
l_3	0.186877	1.000000	3.850528
l_4	15.079223	1.000000	4.649170
l_2^{off}	-0.006796979	1.000000	3.768487
SL model with rescaled b_{21}			
l_1	-7.570518	0.426760	2.722735
l_2	12.705522	-1.269732	3.768487
l_3	0.186877	1.000000	3.850528
l_4	10.555456	1.000000	4.649170
l_2^{off}	-4.757186	1.000000	3.768487

package was used to evaluate the isotropic magnetic exchange interaction parameters [26, 27] considering the fully relativistic LKAG-based method [28]. Fully relativistic calculations employing VASP relaxed structure parameters consider the xc-potential of PBE 1996 [25] and Perdew Wang 1992 [29], $25 \times 25 \times 25$ k -mesh, and energy convergence was better than 10^{-10} Ry.

Spin-lattice model simulations were performed within the LAMMPS package [22], where the above-introduced tetragonal spin-lattice model was implemented in the LAMMPS spin package [12]. In the simulations, a FePt interatomic potential of the MEAM type [30] was considered as well as a custom interatomic potential in the reference-free modified embedded atom method (RF-MEAM)[31, 32] framework. The custom RF-MEAM potential was based on the ab-initio VASP results considering 102 distorted L1_0 FePt structures.

IV. SPIN-LATTICE MODEL FOR TETРАГОНАL(I) FePt SYSTEM.

To manifest the behavior of the above proposed SL model for tetragonal systems, the SL model was used to reproduce the magnetoelastic behavior as calculated by ab-initio VASP calculation. Therefore, initially, prior the SL model simulations, elastic and magnetoelastic properties were determined by ab-initio VASP calculations, using relaxed structure parameters in Table I, except the magnetoelastic calculations where the a finer k -mesh was used to achieve a linear behavior of magnetization direction dependent energy difference under small strain ($a=2.722$ Å, $c=3.770$ Å). The obtained lattice parameters, elastic (Table I) and magnetoelastic constants correspond well to the literature [17, 33, 34]. Besides, the ab-initio MCA constants were estimated (Fig. 3), where $K_1=15.805$ MJ/m³, $K_2 \sim 0$ MJ/m³, and $K_3=0.087$ MJ/m³.

The ab-initio calculations provide the following magnitudes of spin magnetic moments: $\mu_S^{Fe}=2.92$ μ_B and $\mu_S^{Pt}=0.31$ μ_B (compare to the value of Ref. [34]), where μ_B denotes the Bohr magneton. Assuming the dipole-

TABLE III. SL model values of MCA constants K_i depending on the type of included pseudo-dipolar interaction l_i . The MCA is applied only to the Fe sublattice in the presented SL model.

\tilde{K}_1 (meV/f.u.)	K_2 (meV/f.u.)	K_3 (meV/f.u.)
18.06475	0.00000	0.01525
SL model with only the l_4 interaction		
-2.75592	0.0000	0.01525
SL model with all l_i interactions		
58.06637	0.00000	0.01525
SL model with rescaled b_{21}		
46.06588	0.00000	0.01525

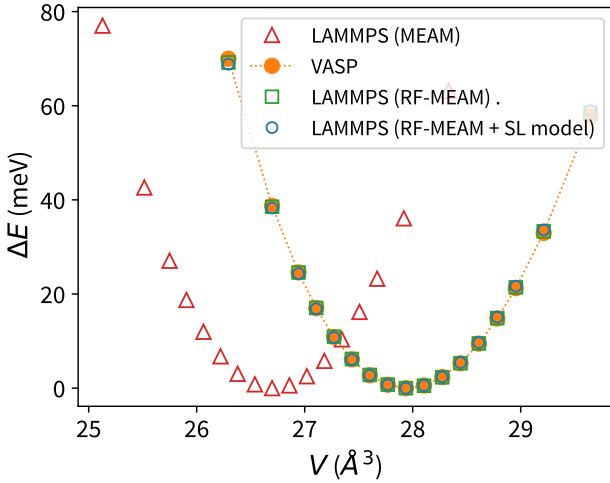


FIG. 2. Volume dependence of the total energy difference in FePt calculations. (filled point) DFT result calculated in VASP. (empty triangle) LAMMPS simulation with an alloy potential. (empty square) LAMMPS simulation with DFT-based potential, (empty circle) LAMMPS simulation with DFT-based potential and SL model included.

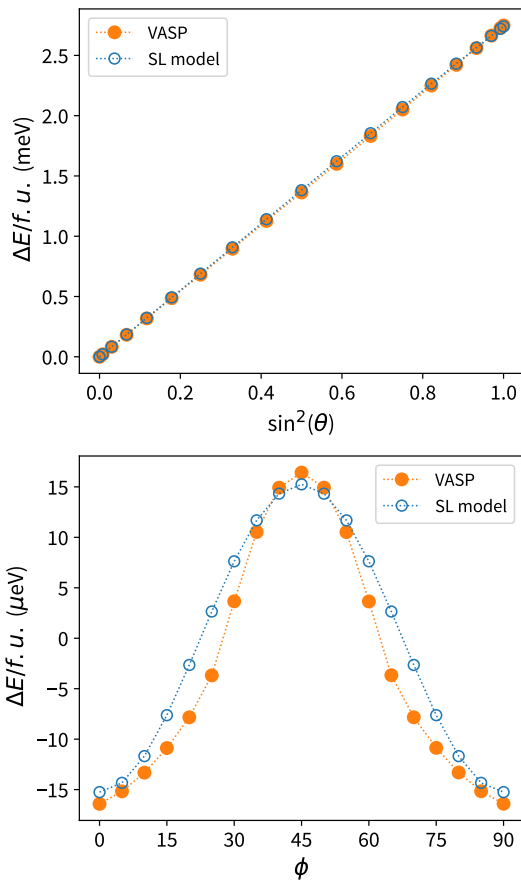


FIG. 3. Magnetocrystalline anisotropy simulation for FePt system obtained by ab initio VASP calculations (filled points) and by the SL-model simulations (empty points).

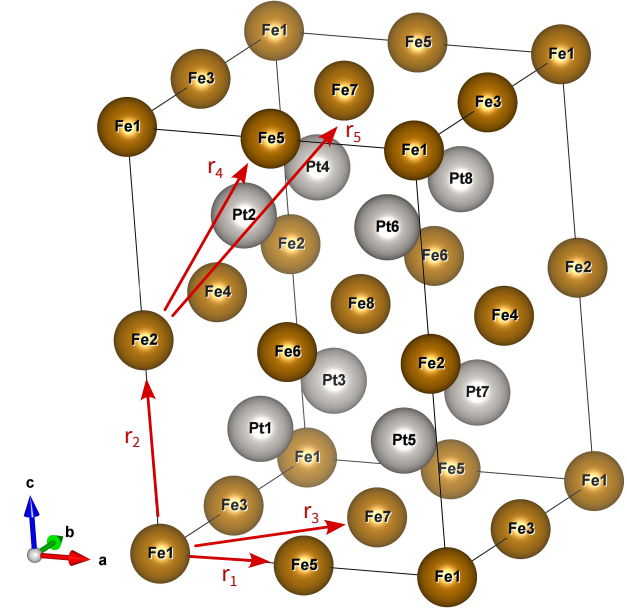


FIG. 4. FePt $2 \times 2 \times 2$ -supercell. Exchange interaction directions for the five nearest Fe-Fe neighbors depicted. (plotted in VESTA 3 [35])

dipole interaction,

$$\mathcal{H}_{dd}(\mathbf{r}, \boldsymbol{\mu}) \propto \left[(\mathbf{e}_{ij} \cdot \boldsymbol{\mu}_i)(\mathbf{e}_{ij} \cdot \boldsymbol{\mu}_j) - \frac{(\boldsymbol{\mu}_i \cdot \boldsymbol{\mu}_j)}{3} \right],$$

where the actual magnitudes of the magnetic moments occur ($\boldsymbol{\mu}_i$ denotes spin moment vector at the site i), unlike the pseudo-dipolar interaction (Eq. 16), the Fe-Pt resp. Pt-Pt dipolar interactions will be one order resp. two orders of magnitude smaller than the dipolar one for Fe-Fe interaction. Therefore, the SL model considers only the Fe sublattice as an approximation. For simplicity, it is applied not only for the pseudo-dipolar interaction but also for the magnetic exchange and MCA interactions (Eq. 13). Otherwise, the pseudo-dipolar interactions of the proposed SL model can be applied separately to the Fe and Pt sublattices, and the same can be used for the MCA interactions.

Building the FePt SL model, initially, the elastic be-

TABLE IV. Bethe-Slater curve parameters for Fe-Fe magnetic exchange interaction $J_i(r_i)$.

	α (meV)	γ	δ (Å)
J_1	10.054688	0.650589	2.722733
J_2	1.450424	0.035201	3.768488
J_3	8.624737	0.262803	3.850526
J_4	-0.280298	6.276936	4.649171
J_5	-3.269634	0.005610	5.387770

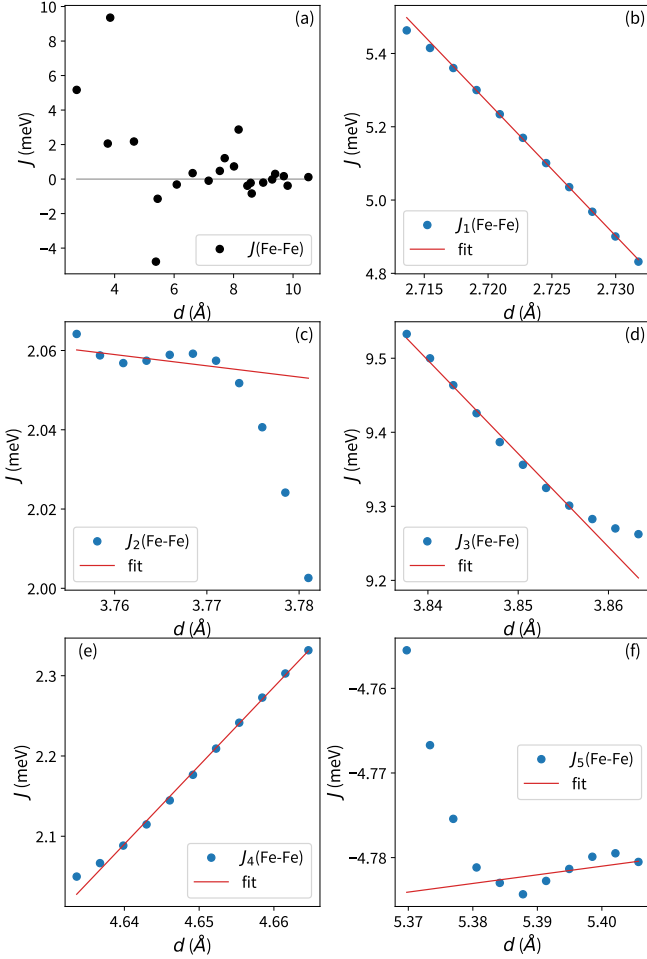


FIG. 5. FePt magnetic exchange coupling parameters. (a) radial dependance of the exchange coupling $J(d)$. (b-f) Exchange coupling $J_i(d)$ under volume change of the FePt cell.

havior given only by the interatomic potential was tested by neglecting the magnetic part \mathcal{H}_M in the SL Hamiltonian (Eq. 12). Evaluating the elastic constants by the finite-displacements method and the energy vs. volume curve and their comparison with the ab-initio results (Table I) reveals that the publicly available alloy-based FePt

TABLE V. Magnetoelastic constants of $L1_0$ FePt were obtained either by linear interpolation of the energy versus strain data given either by ab-initio calculations or spin-lattice (SL) model simulation in LAMMPS (Fig. 6).

	VASP		SL model	
	(MPa)	(meV/f.u.)	nonscaled	rescaled
b_{21}	83.62	14.579	20.825	14.825
b_{22}	-44.96	-7.838	-7.837	-7.837
b_3	-12.62	-2.200	-2.199	-2.199
b_4	-44.59	-15.547	-16.105	-16.103
b'_3	76.41	26.644	26.642	26.642

MEAM potential [30] does not reproduce the values with high accuracy. Indeed, it exhibits a significant discrepancy in the elastic constants, particularly, for the C_{12} constant that differs by more than 120%, see Table I. Besides, the equilibrium volume is modified by 4%. Therefore, in the SL model, a custom ab-initio data-based, interatomic potential of RF-MEAM [31] type was developed. It reproduces well the ab initio energy-volume curve (Fig. 2) as well as the elastic constants C_{ij} (Table I).

To mimic the anisotropic magnetoelastic behavior described by the magnetoelastic energy (Eq. 1), pseudo-dipolar interactions $l_i(r_i)$ as derived above (Eq. 21-Eq. 28) were introduced in the SL-Hamiltonian (Eq. 12) based on the ab-initio magnetoelastic constants b_i . It also includes the l_2^{off} interaction to off-set extra term in arising from l_4 interaction parametrization. The pseudo-dipolar interactions $l_i(r_i)$ were described by Bethe-Slater curves (Eq. 15) with parameters given in the Table II. Depending on the included pseudo-dipolar interactions $l_i(r_i)$, the MCA constants (Eq. 35) of the SL model have to be adapted (Table III), namely the leading K_1 (Eq. 36), to offset the contribution of the l_i interactions to provide correct MAE (Fig. 3). As mentioned, for simplicity, the magnetic exchange interaction \mathcal{H}_{ex} (Eq. 12) was included only for the Fe sublattice (up to the the fifth nearest neighbor interaction $J_i(r_i)$ were considered (Fig. 4)), while the Pt ones were neglected. To approximate the radial dependence of the exchange coupling parameters J_i (Eq. 12), a linear interpolation of the J_{ij} volume dependence near the equilibrium volume was performed (Fig 5). Parameterizing the exchange coupling $J_{ij}(r_{ij})$ by Bethe-Slater curves (Eq. 15), parameters α , γ , δ in Table IV were used to describe the exchange interaction \mathcal{H}_{ex} .

Applying pseudo-dipolar interactions $l_i(r_i)$ one by one, the SL-model simulate properly the ab-initio behavior when l_1-l_3 interactions (Fig. 6b-e, diagonal crosses) were used separately from the l_4 (Fig. 6a, stars). The energy versus strain data follow the linear interpolation of the VASP calculated data (Fig. 6, lines). Combining all the l_i interactions together (Fig. 6, crosses), the SL-model start to overestimate the b_{21} parameter as the slope of the SL model data (Fig. 6a, crosses) was steeper than that one of the linear fit. Further a quadratic-like extra contribution occurs for b_{22} data (Fig. 6b, crosses). It suggests an influence of terms beyond the performed approximation of the strain modification of pseudo-dipolar interaction (Eq. 19). To restore the ab initio like magnetoelastic behavior, the VASP calculated b_{21} magnetoelastic constant used for the parametrization of the pseudo-dipolar interactions (Eq. 21-Eq. 28) was arbitrarily scaled by a factor $f_{b21}=0.7$. Employing the SL-model with rescaled l_i interaction, the proper magnetoelastic behavior was mostly restored (Fig. 6, circles). Only a noticeable quadratic contribution was kept in the determination of the b_{22} magnetoelastic constant (Fig. 6b). The values of the magnetoelastic constants b_i determined by linear inter-

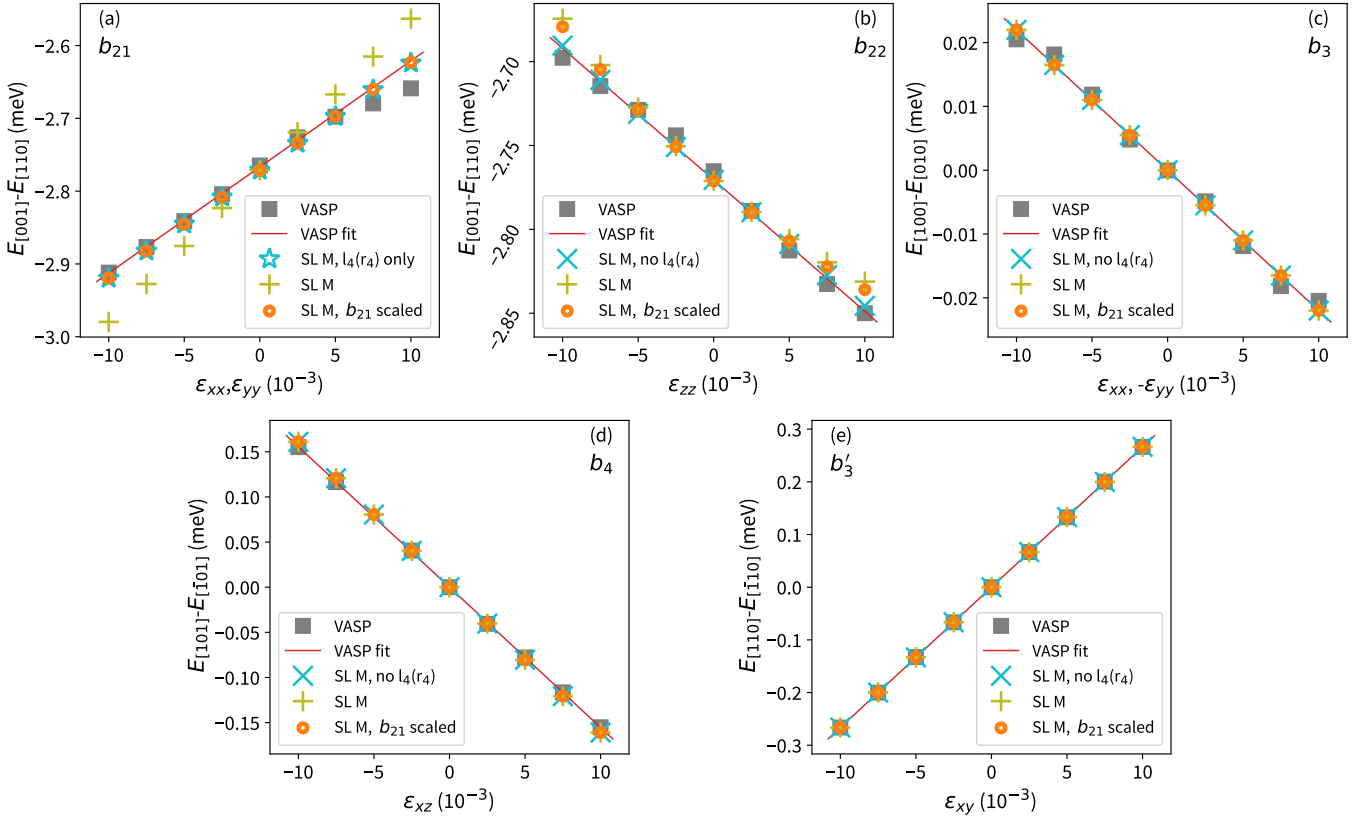


FIG. 6. Energy versus strain data for estimation of the magnetoelastic constants b_i . (square) ab initio VASP results, (lines) linear fit of the VASP results, (star) spin-lattice model (SLM) with only $l_4(r_4)$ interaction included, (crossed diagonal) SLM where $l_4(r_4)$ interaction is excluded, (cross) SLM including all pseudo-dipolar interactions, (circle) SLM with rescaled b_{21} . The direction in the subscripts of the energy axes denotes the direction of the magnetization axis in FM-ordered FePt system.

polation of data from the final rescaled SL-model well correspond to the ab initio values (Table V), with the maximum difference of 3.6% for the b_4 constant.

Further, the proposed SL model reproduces well the MCA behavior following the ab initio MAE data (Fig. 3). Using the properly scaled \tilde{K}_1 constant (Table III), the correct magnitude of the MCA is given by the SL model, irrespective of the l_i interactions included, as manifested by zero strain data in Fig. 6a,b, which provides the energy difference between the [001] and [110] magnetization directions.

V. CONCLUSIONS

In summary, a spin lattice model for tetragonal symmetry was introduced and tested for a representative system of FePt. By analyzing the behavior of the magnetic terms in the spin-lattice Hamiltonian, the parametrization of the magnetic interactions for a tetragonal system was proposed. Namely, a simple model of the pseudo-dipolar interactions reproducing the anisotropic magnetoelastic behavior prescribed by the magnetoelastic energy formula was derived. Including the magnetic ex-

change interaction and magneto-crystalline anisotropy in the spin lattice Hamiltonian, corrections eliminating unwanted interference were proposed.

The derived tetragonal spin-lattice model was implemented in the LAMMPS package and tested for a $L1_0$ FePt – a characteristic representative of tetragonal (I) systems. It was proven that the proposed spin-lattice model reproduces the behavior obtained by ab-initio calculations. In addition, we have developed a custom DFT-based data interaction potential for spin-lattice simulations that describes the energy-volume as well as the elastic constants (C_{ij}) with much higher accuracy than before.

VI. ACKNOWLEDGEMENTS

This work has been supported by GAČR project 24-11388I of the Grant Agency of Czech Republic and by the Ministry of Education, Youth and Sports of the Czech Republic through the e-INFRA CZ (ID:90254)

AUTHOR CONTRIBUTIONS

JŠ: Conceptualization, Methodology, Software, Data curation, Formal analysis, Investigation, Visualization,

Writing – original draft; **DL:** Formal analysis, Writing – review & editing

[1] S. Chikazumi, *Physics of Ferromagnetism*, International Series of Monographs on Physics (OUP Oxford, 2009).

[2] G. Baghdasaryan and Z. Danoyan, in *Magnetoelastic Waves* (Springer Singapore, Singapore, 2018).

[3] Y. Nishibe, Y. Nonomura, K. Tsukada, M. Takeuchi, M. Miyashita, and K. Ito, Determination of engine misfiring using magnetoelastic torque sensor, *IEEE Transactions on Instrumentation and Measurement* **47**, 760 (1998).

[4] I. Garshelis and C. Jones, Miniaturized magnetoelastic torque transducers, *IEEE Transactions on Magnetics* **35**, 3649 (1999).

[5] A. Beskok and A. R. Srinivasa, Simulation and analysis of a magnetoelastically driven micro-pump, *Journal of Fluids Engineering* **123**, 435 (2000), https://asmedigitalcollection.asme.org/fluidsengineering/article-pdf/123/2/435/5590470/435_1.pdf.

[6] C. Petridis, P. Dimitropoulos, and E. Hristoforou, A new magnetoelastic device for sensing applications, *Sensors and Actuators A: Physical* **129**, 131 (2006), eMSA 2004.

[7] B. Spetzler, C. Bald, P. Durdaut, J. Reermann, C. Kirchhoff, A. Teplyuk, D. Meyners, E. Quandt, M. Höft, G. Schmidt, and F. Faupel, Exchange biased delta-e effect enables the detection of low frequency pt magnetic fields with simultaneous localization, *Scientific Reports* **11**, 5269 (2021).

[8] F. T. Calkins, A. B. Flatau, and M. J. Dapino, Overview of magnetostrictive sensor technology, *Journal of Intelligent Material Systems and Structures* **18**, 1057 (2007), <https://doi.org/10.1177/1045389X06072358>.

[9] A. Bieńkowski and R. Szewczyk, The possibility of utilizing the high permeability magnetic materials in construction of magnetoelastic stress and force sensors, *Sensors and Actuators A: Physical* **113**, 270 (2004), new materials and Technologies in Sensor Applications, Proceedings of the European Materials Research Society 2003 - Symposium N.

[10] I. Stockem, A. Bergman, A. Glensk, T. Hickel, F. Körmann, B. Grabowski, J. Neugebauer, and B. Alling, Anomalous phonon lifetime shortening in paramagnetic crn caused by spin-lattice coupling: A combined spin and ab initio molecular dynamics study, *Phys. Rev. Lett.* **121**, 125902 (2018).

[11] J. R. Cooke and J. R. Lukes, An implicit spin lattice dynamics integrator in lammps, *Computer Physics Communications* **271**, 108203 (2022).

[12] J. Tranchida, S. Plimpton, P. Thibaudeau, and A. Thompson, Massively parallel symplectic algorithm for coupled magnetic spin dynamics and molecular dynamics, *Journal of Computational Physics* **372**, 406 (2018).

[13] P. Nieves, J. Tranchida, S. Arapan, and D. Legut, Spin-lattice model for cubic crystals, *Phys. Rev. B* **103**, 094437 (2021).

[14] I. Kornienko, P. Nieves, A. Fraile, R. Iglesias, and D. Legut, Computational study of elastic waves generated by ultrafast demagnetization in fcc ni, *Phys. Rev. Res.* **6**, 023311 (2024).

[15] I. Kornienko, P. Nieves, and D. Legut, Understanding change in the sound wave frequency in a ferromagnet under magnetic field influence (Simon effect) in the low-field regime, *Results in Physics* **73**, 108264 (2025).

[16] P. Nieves, S. Arapan, S. Zhang, A. Kadzielawa, R. Zhang, and D. Legut, Maelas 2.0: A new version of a computer program for the calculation of magneto-elastic properties, *Computer Physics Communications* **271**, 108197 (2022).

[17] D. Legut and P. Nieves, Second-order anisotropy due to magnetostriction for L10-FePt, *Solid State Sciences* **160**, 107782 (2025).

[18] P. Ravindran, A. Kjekshus, H. Fjellvåg, P. James, L. Nordström, B. Johansson, and O. Eriksson, Large magnetocrystalline anisotropy in bilayer transition metal phases from first-principles full-potential calculations, *Phys. Rev. B* **63**, 144409 (2001).

[19] P. Nieves, S. Arapan, S. Zhang, A. Kadzielawa, R. Zhang, and D. Legut, Maelas: Magneto-elastic properties calculation via computational high-throughput approach, *Computer Physics Communications* **264**, 107964 (2021).

[20] S. Zhang and R. Zhang, Aelas: Automatic elastic property derivations via high-throughput first-principles computation, *Computer Physics Communications* **220**, 403 (2017).

[21] P. Nieves, S. Arapan, S. Zhang, A. Kadzielawa, R. Zhang, and D. Legut, Automated calculations of exchange magnetostriction, *Computational Materials Science* **224**, 112158 (2023).

[22] A. P. Thompson, H. M. Aktulga, R. Berger, D. S. Bolineanu, W. M. Brown, P. S. Crozier, P. J. in 't Veld, A. Kohlmeyer, S. G. Moore, T. D. Nguyen, R. Shan, M. J. Stevens, J. Tranchida, C. Trott, and S. J. Plimpton, LAMMPS - a flexible simulation tool for particle-based materials modeling at the atomic, meso, and continuum scales, *Comp. Phys. Comm.* **271**, 108171 (2022).

[23] G. Kresse and J. Furthmüller, Efficient iterative schemes for ab initio total-energy calculations using a plane-wave basis set, *Phys. Rev. B* **54**, 11169 (1996).

[24] G. Kresse and D. Joubert, From ultrasoft pseudopotentials to the projector augmented-wave method, *Phys. Rev. B* **59**, 1758 (1999).

[25] J. P. Perdew, K. Burke, and M. Ernzerhof, Generalized gradient approximation made simple, *Phys. Rev. Lett.* **77**, 3865 (1996).

[26] J. M. Wills, M. Alouani, P. Andersson, A. Delin, O. Eriksson, and O. Grechnyev, The full-potential electronic structure problem and RSPt, in *Full-Potential Electronic Structure Method: Energy and Force Calculations* (Springer Berlin Heidelberg, Berlin, Heidelberg, 2010) pp. 47–73.

- [27] Y. O. Kvashnin, O. Gränäs, I. Di Marco, M. I. Katsnelson, A. I. Lichtenstein, and O. Eriksson, Exchange parameters of strongly correlated materials: Extraction from spin-polarized density functional theory plus dynamical mean-field theory, *Phys. Rev. B* **91**, 125133 (2015).
- [28] A. Szilva, Y. Kvashnin, E. A. Stepanov, L. Nordström, O. Eriksson, A. I. Lichtenstein, and M. I. Katsnelson, Quantitative theory of magnetic interactions in solids, *Rev. Mod. Phys.* **95**, 035004 (2023).
- [29] J. P. Perdew and Y. Wang, Accurate and simple analytic representation of the electron-gas correlation energy, *Phys. Rev. B* **45**, 13244 (1992).
- [30] J. Kim, Y. Koo, and B.-J. Lee, Modified embedded-atom method interatomic potential for the Fe–Pt alloy system, *Journal of Materials Research* **21**, 199 (2006).
- [31] A. I. Duff, M. Finnis, P. Maugis, B. J. Thijssse, and M. H. Sluiter, MEAMfit: A reference-free modified embedded atom method (RF-MEAM) energy and force-fitting code, *Computer Physics Communications* **196**, 439 (2015).
- [32] R. J. Slooter, M. H. F. Sluiter, W. G. T. Kranendonk, and C. Bos, A reference-free MEAM potential for α -Fe and γ -Fe, *Journal of Physics: Condensed Matter* **34**, 505901 (2022).
- [33] P. Ravindran, A. Kjekshus, H. Fjellvåg, P. James, L. Nordström, B. Johansson, and O. Eriksson, Large magnetocrystalline anisotropy in bilayer transition metal phases from first-principles full-potential calculations, *Phys. Rev. B* **63**, 144409 (2001).
- [34] Z. Lu, R. V. Chepulskii, and W. H. Butler, First-principles study of magnetic properties of $L1_0$ -ordered MnPt and fept alloys, *Phys. Rev. B* **81**, 094437 (2010).
- [35] K. Momma and F. Izumi, *VESTA3* for three-dimensional visualization of crystal, volumetric and morphology data, *Journal of Applied Crystallography* **44**, 1272 (2011).